International Journal of Biotech Trends and Technology
ISSN: 2249 – 0183 /doi:10.14445/22490183/IJBTT-V11I1P602

Volume 11 Issue 1, 7-15, Jan-Mar 2021

Video-based Photoplethysmography and Machine Learning Algorithms to Achieve Pulse Wave Velocity

Pedro Henrique de Brito Souza[#1], Israel Machado Brito Souza[*2], Symone Gomes Soares Alcalá[#3], Priscila Valverde de Oliveira Vitorino[*4], Adson Ferreira da Rocha[#1], Talles Marcelo Gonçalves de Andrade Barbosa[*4,#5]

[#1] *Graduate Program in Biomedical Engineering, University of Brasília, Brasília/DF, 72.444-240, Brazil*
[*2] *Department of Computer Science, University of Porto, Porto, 4169-007, Portugal*
[#3] *Graduate Program in Production Engineering, Federal University of Goiás, Aparecida de Goiânia/GO, 74.968-755, Brazil*
[*4] *Graduate Program in Health Care, Pontifical Catholic University of Goiás, Goiânia/GO, 74.605-010, Brazil*
[#5] *School of Exact Sciences and Computing, Pontifical Catholic University of Goiás, Goiânia/GO, 74.605-010, Brazil*

Abstract *— The pulse transit time (PTT) is commonly used to monitor pulse wave velocity (PWV). In general, the instruments of signal acquisition, from which these physiological variables are estimated, require a contact surface for the sensors' installation and positioning, such as an inflatable cuff, creating a restriction or obstruction to the users' movement and ergonomics. This paper describes the development and evaluation of a contactless cardiovascular monitor, which can measure the PTT and PWV by analyzing the photoplethysmographic (PPG) signal obtained by an RGB camera's green channel, i.e., without using sensors in contact with the skin. This monitor requires the PPG signal acquisition of two different regions of interest simultaneously: the forehead and right-hand palm. The time differences between two critical points of PPG signals were used to input machine learning algorithms, alongside other input features, such as user's gender, height, and weight, to estimate Aortic PTT. The proposed monitor was tested by comparing its measurements of 36 healthy volunteers to the CARDIOS Dyna-MAPA+, gold standard equipment for these physiological variables measurement, showing a Pearson correlation coefficient of approximately 0.77 and a mean squared error of* 0.104×10^{-3} *for Aortic PTT.*

Keywords — *Blood Pressure, Camera, Machine Learning, Pulse Transit Time, Pulse Wave Velocity, Contactless.*

This study was supported by FAPEG (in Portuguese, Fundação de Amparo à Pesquisa do Estado de Goiás), and CAPES (in Portuguese, Coordenação de Aperfeiçoamento de Pessoal de Nível Superior).

I. INTRODUCTION

Pulse transit time (PTT) is when blood pressure or flow wave takes to propagate between two arterial sites [1]. It is inversely correlated to pulse wave velocity (PWV) and can be measured by the relative timing between proximal and distal pulsatile waveforms [2]. PWV refers to the velocity at which the pulse wave flows through the blood vessels. Some methods used to measure PWV require non-invasive instruments that must use an inflatable cuff (auscultation, oscillometric, and volume clamping methods, for example) attached to the body, making people feel uncomfortable [3]. Normally, the acquisition of PTT is made using the moment when the R-peak of an electrocardiography (ECG) signal occurs when the maximum slope of a PPG occurs [16]. However, according to Mukkamla et al. [4], this type of acquisition returns the pulse arrival time (PAT), which is composed of the sum of the PTT and the pre-ejection period (PEP). Studies found that PTT can be measured by the time interval between a specific point of two PPG signals positioned in two different body sites to avoid PEP [13], [24]. Considering that PTT values can be measured using two photoplethysmography sensors in different body sites, the same approach can be applied using a camera to acquire the photoplethysmography signal. In the study developed by Khong et al. [14], the chest and forehead were the selected body sites, considering the chest as the proximal region or the blood pulse origin and the forehead as the distal region. However, according to Sugita et al. [9], the pulse time difference between the forehead and the right-hand palm was the most correlated one compared to the systolic blood pressure measured by the reference sensor attached to the left middle finger of a person.

According to McDuff et al. [5][6], it is possible to acquire the PPG signal using a digital camera and ambient light, as shown in Fig. 1. This contactless technique consists of acquiring the PPG signal by detecting the blood volume pulse (BVP) variation in the user's skin, which is caused by the heartbeats, through the reflected light in the human skin [7][8]. According to Sugita et al. [9], the PTT can also be measured by analyzing the PPG signal acquired by a contactless technique. The contactless PTT measurement allows a way to measure the PWV without wearing an inflatable cuff and has a continuous measurement without an invasive sensor. It also allows the self-measurement at

home, avoiding environmental factors that can lead to inaccurate results (e.g., white coat effect).

Studies pointed that self-measurement of physiological variables at home with a certain routine is better than measuring them at hospitals [10], justifying the attention gained from experts to control the progress of diseases, such as hypertension [11]. Besides, this technique would also allow the external monitoring of a person's condition, exploring the concept of remote sensors and telemedicine [12].

A video-based photoplethysmography technique was developed using two different regions of interest (ROI) simultaneously to recover the contactless measurement signals. Thus, this paper's main purpose is to propose an efficient and flexible software to measure the PTT and PWV based on empirical methods. The proposed software uses an algorithm to process and analyzes the video, detecting the PPG signal's critical points, as shown in Fig. 2.

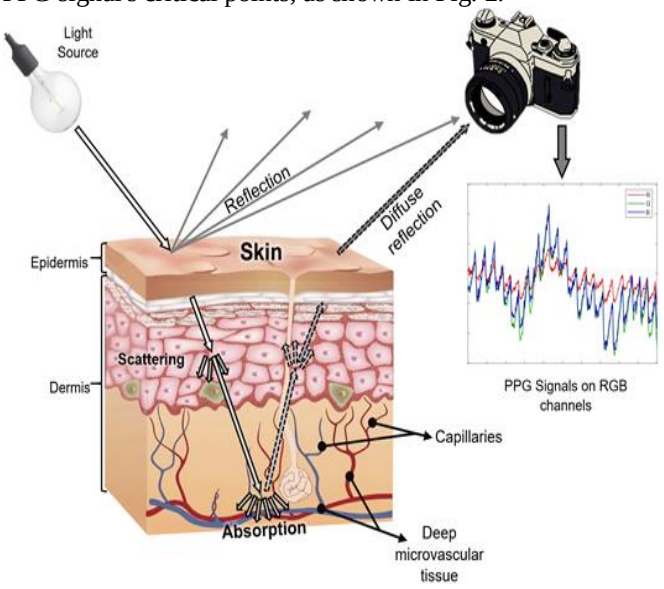

Figure 1. Contactless PPG signal acquisition.

A smart peak detection algorithm matches the critical points created by the same heartbeat in the PPG signals of the two ROIs.

The mean time difference (Δt) only exists because of the time delay between two critical points of BVPs, which reach the ROIs according to the distance between the heart and each ROI. To ensure the best possible results in estimating the Aortic PTT values, the tests are performed by including seven physiological variables (gender, height, age, weight, Body Mass Index (BMI), Body Surface Area (BSA), and Δt) as inputs for machine learning techniques, which were responsible for estimating the Aortic PTT.

This paper is organized as follows. In Section 2, the proposed technique to acquire the Δt and the environment test setup is described. The results for 36 different volunteers over a broad range of skin-types, according to the Fitzpatrick scale [25], are presented at the end of Section 2. Section 3 presents the performance of machine learning algorithms to evaluate their performance in estimating the Aortic PTT. The results comparing the contactless software technique to the gold standard equipment for PWV measurement showed a high correlation between the PTT and PWV results, attesting to the proposed technique's efficiency. Finally, the conclusion is presented in Section 4.

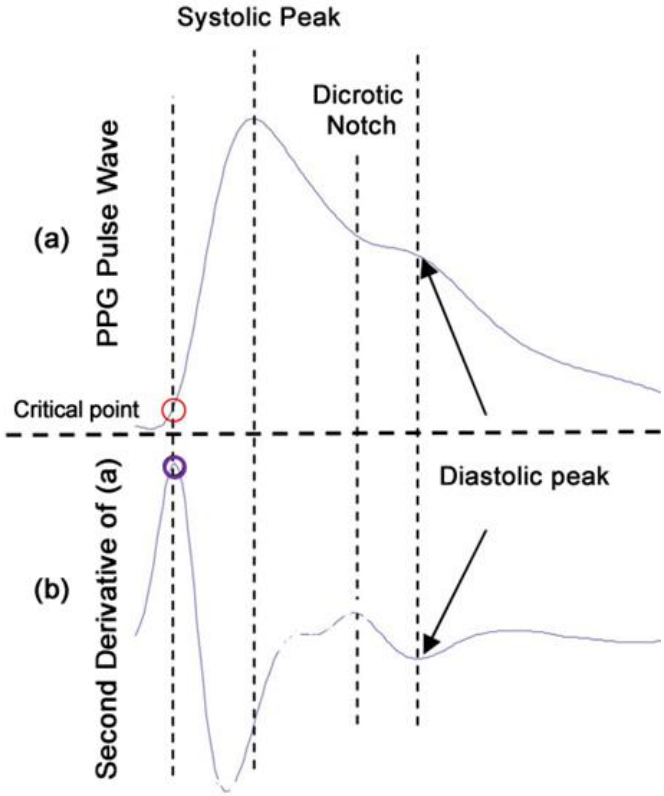

Figure 2. The critical point (red O) on PPG signal (a), obtained by detecting peaks in the second derivation (b) of the PPG signal, is an event that marks the beginning of systole (purple O). The beginning of systole is the event used to mark the moment that BVP reaches the ROI.

II. MATERIALS AND METHODS

A. Mean Time Differences (Δt) *Acquisition*

The proposed software performs the video processing and the contactless PPG acquisition. The process is described in Fig. 3. The ROI was selected into RGB channels, but only the green channel was used because its light wavelength is absorbed more efficiently by the blood's hemoglobin. The BVP peaks are directly related to the hemoglobin content [17-19]. The mean of each green channel frame's pixels, on both ROIs, was used to form the raw signal x[n].

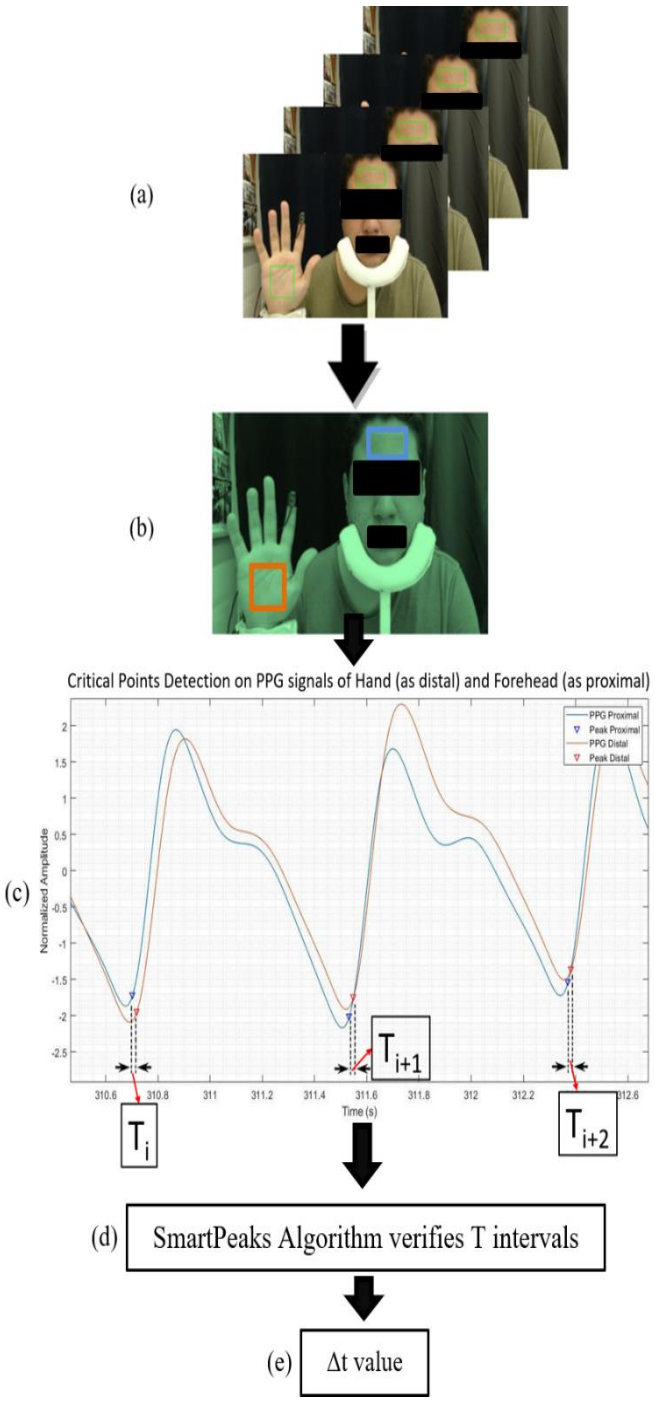

Figure 3. Time intervals between critical points in two different ROIs (T). (a) Getting the ROIs within the frames; (b) Green channel is selected as the fixed color channel; (c) Raw signals (blue signal is the Forehead proximal PPG, and the orange signal is the Hand distal PPG); the critical point detection in the filtered signals, corresponding to the beginning of systole, as shown in Figure 2; (d) SmartPeaks Detection Algorithm, as shown in Figures 4 and 5; and (e) Δt in seconds (this variable is described by Equation 2, as the arithmetic means of T).

Then, a detrending technique filter, based on a smoothness priors approach [20-21], filtered x[n], removing the low frequencies (< 0.3 Hz), usually caused by the user's movement. After filtering x[n], the raw green channel was normalized by subtracting its mean and dividing by its standard deviation, as shown in equation (1),

$$z[n] = (x[n] - \mu) \div \sigma \quad (1)$$

where μ and σ are the mean and the standard deviation of x[n], respectively.

A 15th order Butterworth bandpass filter was used to filter z[n] with the low and high frequency of 0.75 Hz – 4 Hz. It is capable of acquiring photoplethysmography signals from 45 to 240 beats per minute (bpm). The fixed color technique's resulting signal is similar to the photoplethysmography signal acquired by a contact PPG sensor; however, this signal is the PPG obtained by a contactless technique [26]. The signals acquired by the camera were obtained at 30 Hz, so a cubic spline interpolation was applied in the signals to interpolate them to 500 Hz. A custom peak detection algorithm is applied to the filtered z[n] signals, detecting all critical points present in both ROIs' PPG signals.

As shown, two types of filters are used to reduce the noise in the PPG signal. However, in some cases, the filters cannot remove the noise completely, which might make critical point detection more difficult. Then, to avoid the possibility of a critical point appears on the signal of an ROI and not on the other, due to the noise, the described heuristic in Fig. 4 was applied to match the critical peaks between these signals. For every critical point found on a signal, the software searches for a critical point on the other signal, between ± 0.05 seconds of the time difference (T). If found, the software considers that these critical points correspond to the same systole, as shown in Fig. 4, and saves them as an element of T to be further the input of equation (2) [14],

$$\Delta t = (|T_1| + |T_2| + |T_3| + \ldots + |T_N|) \div N \quad (2)$$

where T is the time intervals between the critical points and N is the number of valid critical points on ROIs.

B. Test Environment and Preliminary Results

The experiment was conducted in a laboratory with a controlled environment. The laboratory temperature was set to 24°C (75°F), and its luminosity was set to 250 Lux. The experiment inclusion and exclusion criteria allowed 36 different volunteers (17 men and 19 women) to participate. According to the Fitzpatrick scale, the volunteers were 19 to 29 years old, with different skin color types [25]. They were seated at approximately 45 cm from the camera. A Logitech, Inc. HD Pro Webcam C920 camera was used in the experiment with an i7 Intel® Core™ 8GB RAM computer running MATLAB (The Mathworks, Inc.) R2018a software on Windows 10 (Ver. 20H2). A 5 minutes video was recorded and processed in real-time at 30 frames per second (fps) and 800x448 resolution (16:9 Aspect Ratio).

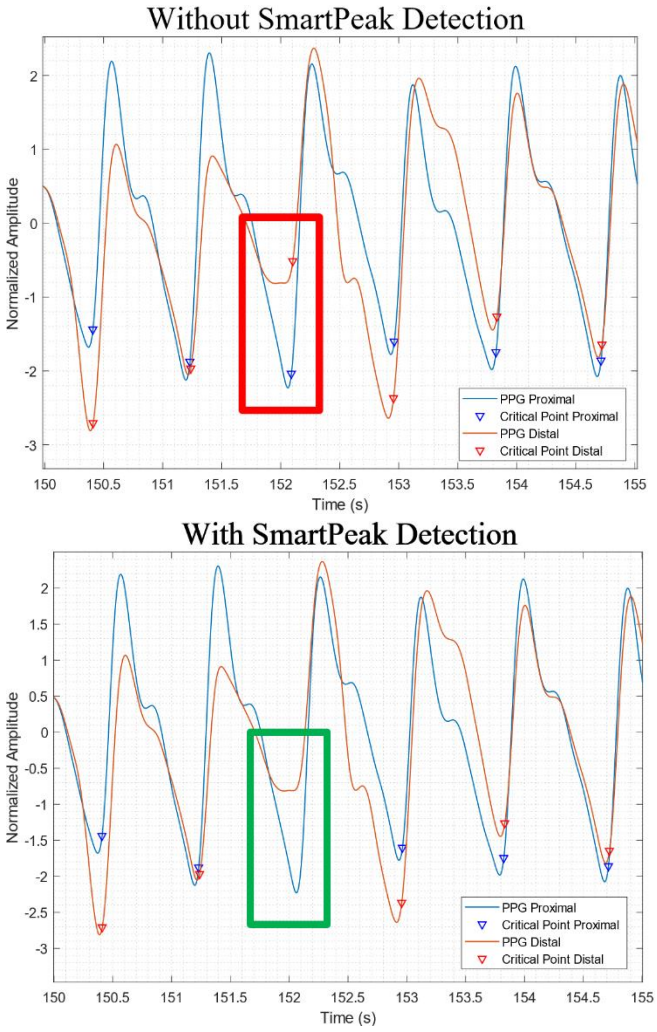

Figure 4. Smartpeak detection matching the critical correspondent points of different ROIs. The orange line is the signal acquired in the Hand, and the blue line is the signal acquired in the forehead. In the first plot, the red rectangle shows the critical point that does not have a correspondent one in the other signal. The green rectangle in the second plot shows the invalid critical point, which is removed from T.

During the video recording, the standard gold instrument was used to reference the contactless PWV measurements. The equipment was the CARDIOS® Dyna-MAPA+, an ambulatory blood pressure monitoring with a cuff wrapped to the volunteer's left upper arm to acquire the PWV.

The contactless PTT measurement technique was implemented in MATLAB software, allowing a good performance during the signal processing. First, it was utilized the Computer Vision System Toolbox to identify and track the volunteer's face. Thus, only the forehead was selected to compose the first ROI. The volunteers were asked to place their palms in a fixed square drawn on the screen to get the second ROI.

1. **Input**: The PPG signals of Forehead and Hand
   ppg_Forehead = mean(green_pixels(roiForehead));
   ppg_Hand = mean(green_pixels(roiHand));
2. **Initialization phase**:
   a) All PPG critical points are selected on both ROIs, including the unpaired ones (Fig. 4 – Red rectangle)
   [pF, lF] = findpeaks(ppg_Forehead);
   [pH, lH] = findpeaks(ppg_Hand);
   where pF and pH have the points amplitudes and lF and lH have the peaks locations (time)
   b) For the database, timeDiff = 0.05 second (This value was determined based on the comparison of Δt and the reference PTT).
3. **Smart Peak Detection phase** (Fig. 4 – Green rectangle)
   a) Detect difference between the number of critical points of ppg_Forehead and ppg_Hand:
   sizeDiff = absolute(size(lF) - size(lH));
   b) Detect the PPG with more points:
   if size(lH) ≤ size(lF)
   then call function
   pttVectors(lH,pH,lF,pF,sizeDiff,timeDiff);
   else
   then call function
   pttVectors(lF,pF,lH,pH,sizeDiff,timeDiff);
   end
   The pttVectors function compares the point i of the smallest array within the point j of the biggest array, varying between j = i - sizeDiff to j = i + sizeDiff. When a point is found in the biggest array and its time difference to the i correspondent in the smallest array is smaller than timeDiff, the function assumes that they match, creating the time differences (T) array.
4. **Calculate Δt according to the Equation 2.**

Figure 5. SmartPeaks Detection Algorithm is responsible for matching the critical points.

Before starting the contactless measurement using the camera, the volunteers wore the Dyna-MAPA+ inflatable cuff on the left arm. To avoid noise caused by movements, they were asked to sit still, place the head and the right arm in custom bracing, and look at the camera while the video was being recorded and analyzed simultaneously. Fig. 6 shows an example of the experiment setup. The files containing the results were analyzed after the video recording. The Dyna-MAPA+ gave the reference Aortic PTT, and its results were compared to the PTT values obtained by the camera once the process was done with all volunteers.

The mean time difference (Δt) was used as input of machine learning algorithms, alongside other input features, such as user's height and weight, to estimate the contactless Aortic PTT. Table I and Table II show results.

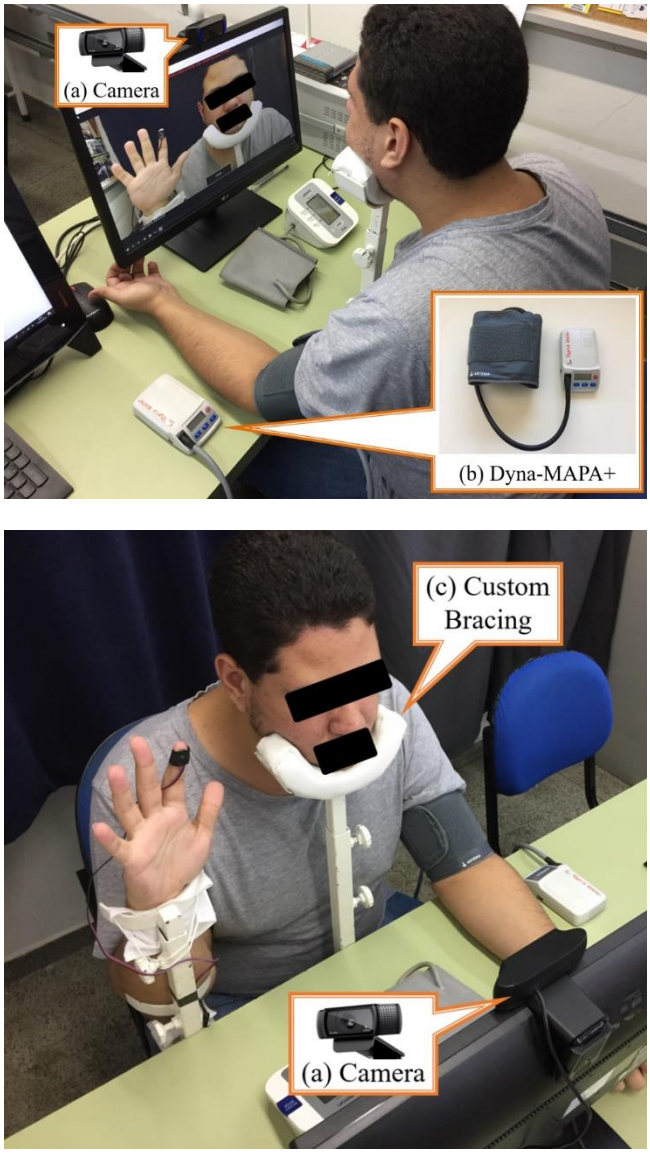

Figure 6. (a) Logitech, Inc. HD Pro Webcam C920 at 45 cm from the volunteer. (b) Dyna-MAPA+ next to the volunteer wrapping the inflatable cuff. (c) Custom bracing to avoid the volunteer's movement during the signal acquisition.

III. MACHINE LEARNING ALGORITHMS TO ESTIMATE AORTIC PTT USING TIME DIFFERENCES

This section presents machine learning algorithms' performance in estimating the Aortic PTT values given by the Dyna-MAPA+ (in the form of PTT = 1/PWV) [15]. First, the data set is described; then, the machine learning algorithms' results are presented and compared. The simulations have been performed on the MATLAB environment, running on a PC equipped with an Intel Core i7-4700MQ 2.4GHz-3.4GHz processor of 4 cores and 8GB of RAM.

A. Data Set Description

Once the process was done with all volunteers, the files containing the results, which were saved during the video recording, were compared to the reference sensor's PTT values. A preliminary data set for machine learning purposes was created. It has the 36 volunteers' data and consists of seven input variables and one output variable (Aortic PTT). The input variables are gender, height, age, weight, Body Mass Index, Body Surface Area, and meantime difference (Δt), as described in Table III.

The Forward Sequential Feature Selection method (FSFS) method was applied to evaluate the input variables' relevance and eliminate redundant variables. It is a simple and fast (the time complexity is $O(d^2)$) approach [22]; and selects the best subset of features (variables) by sequentially including features until there is no improvement in prediction, using a hill-climbing search strategy.

The FSFS method was performed in 100 independent runs using 10-fold cross-validation, as illustrated in Fig. 7. The results show that features 1 (gender), 2 (height), and 7 (Δt) were selected in all the runs, revealing that these features are important in estimating the output variable. On the other hand, features 4 (weight) and 5 (BMI) were selected in 32 and 25 runs, respectively; while, features 3 (age) and 6 (BSA) were selected in few runs (0 and 2, respectively). Possibly, feature 3 (age) was not selected due to the small variation of the volunteers' ages.

According to results, features 1, 2, 4, and 7 were employed as input variables and Aortic PTT as an output variable for designing the learning models in this paper. After that, the data set was divided into three datasets: the training dataset (65%), the validation dataset (15%), and the testing dataset (20%).

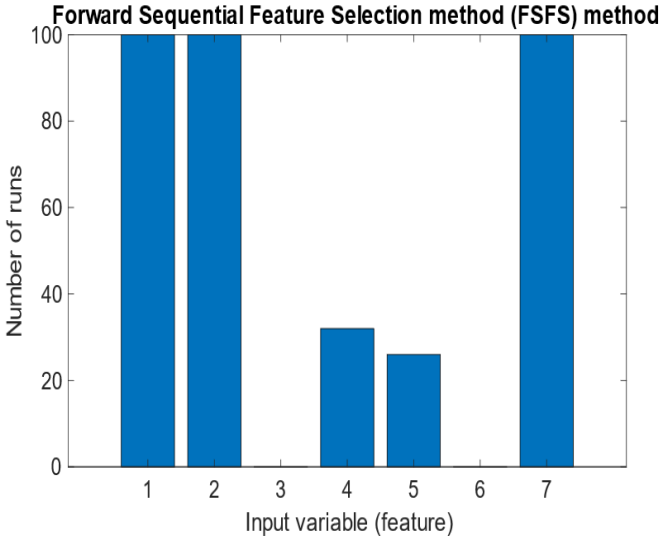

Figure 7. Feature selection using the FSFS method in 100 independent runs.

TABLE I. ΔT RESULTS FOR 17 MEN

Volunteer ID	Height (cm)	Age	Weight (kg)	BMI (kg/m²)	Time differences (Δt) in seconds
1	174	26	64	21.0	0.0231
2	182	24	64	19.4	0.0215
3	172	21	76	25.7	0.0450
4	172	22	78	26.3	0.0486
5	181	23	71	21.6	0.0367
6	173	22	72	24.0	0.0254
7	171	21	70	23.9	0.0211
8	189	23	68	19.1	0.0308
9	173	23	62	20.7	0.0273
10	167	20	70	25.0	0.0274
11	187	25	77	22.1	0.0187
12	173	26	76	25.6	0.0197
13	174	22	84	27.7	0.0300
14	169	22	52	18.3	0.0402
15	168	23	89	31.5	0.0207
16	184	23	99	29.2	0.0125
17	171	29	63	21.6	0.0305

TABLE II. ΔT RESULTS FOR 19 WOMEN

Volunteer ID	Height (cm)	Age	Weight (kg)	BMI (kg/m²)	Time differences (Δt) in seconds
1	176	25	70	22.4	0.0164
2	156	23	55	22.5	0.0411
3	159	19	50	19.9	0.0283
4	156	20	49	20.2	0.036
5	164	23	60	22.3	0.0402
6	155	24	44	18.1	0.0251
7	169	21	53	18.7	0.2840
8	158	20	62	24.6	0.0247
9	157	25	60	24.2	0.0395
10	155	28	44	18.4	0.0275
11	154	27	53	22.3	0.0219
12	150	22	60	26.7	0.0324
13	162	20	70	26.9	0.0143
14	163	21	67	25.2	0.0294
15	174	19	54	17.9	0.0133
16	166	24	58	20.9	0.0205
17	154	21	50	21.0	0.0291
18	162	20	56	21.1	0.0310
19	162	24	78	29.8	0.0218

TABLE III. INPUT VARIABLES DESCRIPTION

Input variable number	Input variable description	Unit	Min. value	Max. value	Mean value
1	Gender	-	0	1	0.527
2	Height	cm	150	189	167.555
3	Age	year	19	29	22.805
4	Weight	kg	44	99	64.666
5	Body Mass Index (BMI)	kg/m^2	17.900	31.500	22.938
6	Body Surface Area (BSA)	m^2	1.400	2.200	1.727
7	Δt	second	0.012	0.048	0.027

B. Learning Models Description and Setup

In this work, tests are performed by comparing the following learning models: Levenberg-Marquardt Backpropagation (LMB), Extreme Learning Machine (ELM), Ensemble of Levenberg-Marquardt Backpropagation (ELMB), and Ensemble of Extreme Learning Machine (EELM). The single learning model, i.e., LMB and ELM, are implemented as follows:

- LMB: using trainlm network training function of the Neural Network Toolbox in MATLAB, where the parameters are set to the default values; and
- ELM: standard ELM, implemented as the paper [23], with sigmoid as the activation function.

For each learning model and each component-model of an ensemble system, the number of neurons in the hidden layer L is selected by varying it in the interval [1, 20]. And for each model, L's value is chosen based on the lowest mean squared error on 10-fold cross-validation using the training data set, where the best value of L is selected as the one that minimizes the mean testing error on the 10-folds [23]. It

should be pointed out that each model is designed using the training dataset. Experiments are also performed by comparing the effectiveness of ELMB and EELM, which are implemented as follows:

- ELMB: 20 NN models trained with the LMB algorithm, where the models' outputs are combined by average; and
- EELM: 20 NN models trained with the standard ELM algorithm, where the models' outputs are combined by average.

The learning models are evaluated using the mean and standard deviation of the Mean Squared Error (MSE), the Root Mean Squared Error (RMSE), the Mean Absolute Error (MAE), and the Pearson Correlation Coefficient (PCC) between the predicted outputs and the real outputs on the data sets. In the experiments, only the error on the testing data set is reported.

C. Comparison of Learning Models

In this section, LMB, ELM, ELMB, and EELM are compared. The aim is to evaluate their performances in estimating the Aortic PTT. For this purpose, for each model, the results are averaged over 20 runs. The errors on the testing dataset and the processing time (in seconds) of each learning model are presented in Table IV.

For the single learning models (LMB and ELM), it has been observed that ELM outperforms LMB in terms of errors (e.g., the average MSE for the LMB model is 0.241×10^{-3}; while for the ELM model is 0.167×10^{-3}) and processing time (i.e., the average processing time for the LMB model is 20.953 seconds; while for the ELM model is 2.542 seconds). Moreover, it has been observed that the use of multiple models (ensemble models) reduces the prediction error significantly. For example, for the ensemble of LMB models (i.e., ELMB), the average MSE is 0.124×10^{-3}; and, for the single LMB model, the average MSE is 0.241×10^{-3}. Additionally, for the ELM models' ensemble (i.e., EELM), the average MSE is 0.123×10^{-3}; and, for the single ELM model, the average MSE is 0.167×10^{-3}. It can be observed that EELM and ELMB have similar error values; however, EELM has a lower processing time when compared to ELMB.

In the ELMB model experiments, the lowest MSE error in a run was 0.107×10^{-3}; while for the EELM model, this value was 0.104×10^{-3}. The estimated outputs of the ELMB and the EELM models in the testing dataset are reported in Table V. It can be observed that the estimated outputs are similar to the Aortic PTT's real output values. Table VI shows the values of PWV obtained by the function PWV = 1/PTT.

TABLE IV. AVERAGE AND STANDARD DEVIATION OF THE PREDICTION ERRORS AND PROCESSING TIME OF THE LEARNING MODELS[1].

Learning Model	MSE	RMSE	MAE	PCC	Processing Time (s)
LMB	0.241 (0.170)	0.120 (0.085)	12.770 (4.365)	0.626 (0.255)	20.953 (0.699)
ELM	0.167 (0.065)	0.084 (0.033)	10.823 (2.322)	0.721 (0.107)	**2.5420 (0.050)**
ELMB	0.124 (0.007)	0.062 (0.004)	9.832 (0.339)	**0.769 (0.019)**	411.541 (14.217)
EELM	**0.123 (0.015)**	**0.061 (0.008)**	**9.331 (0.748)**	**0.769 (0.026)**	50.707 (0.682)

[1]The MSE, RMSE, and MAE values have been multiplied by 10^3; Values in parentheses are the standard deviation value in 20 runs, and values outside parentheses are the average value in 20 runs.

TABLE V. PTT REAL OUTPUT AND PREDICTED OUTPUT VALUES OF ELMB AND EELM IN THE TESTING DATA SET.

Output/ Volunteer	Testing sample 1	Testing sample 2	Testing sample 3	Testing sample 4	Testing sample 5	Testing sample 6	Testing sample 7
Real output values (Aortic PTT)	0.1754	0.2326	0.2128	0.2128	0.2128	0.2041	0.2041
Predicted value of ELMB	0.1826	0.2198	0.2162	0.2170	0.2065	0.2191	0.2196
Predicted value of EELM	0.1838	0.2189	0.2100	0.2098	0.2076	0.2174	0.2174

TABLE VI. PWV REAL OUTPUT AND PREDICTED OUTPUT VALUES OF ELMB AND EELM IN THE TESTING DATA SET

Output/ Volunteer	Testing sample 1	Testing sample 2	Testing sample 3	Testing sample 4	Testing sample 5	Testing sample 6	Testing sample 7
Real output values (PWV)	5.7	4.3	4.7	4.7	4.7	4.9	4.9
Predicted value of ELMB	5.4764	4.5496	4.6253	4.6083	4.8426	4.5641	4.5537
Predicted value of EELM	5.4407	4.5683	4.7619	4.7664	4.817	4.5998	4.5998

IV. CONCLUSION AND FUTURE WORK

This paper presented the software to measure the PTT and PWV by analyzing PPG signal waves acquired using a digital camera recording two regions of interest simultaneously. The experiments described in the previous sections showed high agreement between the video-based and the reference acquisition methods, proving that it is possible to accurately measure PPT and PWV using a contactless method with machine learning techniques. The machine learning methods could reduce the error by introducing more physiological variables, such as gender, height, and meantime difference (Δt), in predicting the Aortic PTT. The video-based technique does not require sensors attached to the volunteer's skin, making monitoring the physiological data easier for the user in daily life.

However, some limitations must be addressed in future implementations. The experiments described in this paper were done by asking the volunteers to keep still while recording the video to avoid motion-induced distortions in the signals. Future work will be focused on creating heuristics to handle the noise caused by the volunteer's movements while using the software. The next tasks will also focus on Ubiquitous PWV Monitoring, allowing people to measure their PWV anytime along the day without uncomfortable sensors attached to the body. Considering that the software only needs small segments of video to obtain the mean time difference (Δt) based on the critical points present in the PPG signal, the proposed software will also be able to obtain the PWV through the same segments of video, allowing the detection of abrupt variations and performing more measurements than a standard method, which require contact to the skin.

ACKNOWLEDGMENT

The authors would like to thank for the help and contributions their colleagues Lucas M. da Silva, Gabrielly C. Ramos, José Olímpio Ferreira, Tharcis P. Sacramento, Ana Carolina Arantes, Maicon Borges Euzébio, Thainã M. de Souza, Tátila P. da Silva, Juliana Tavares, Lucas M. Lima, and Sandy M. Lima.

REFERENCES

[1] M. Gao, N. B. Olivier, R. Mukkamala, Comparison of non-invasive pulse transit time estimates as markers of blood pressure using invasive pulse transit time measurements as a reference, Physiological Reports 4 (10). doi:10.14814/phy2.12768

[2] R. Mukkamala, J.-O. Hahn, Toward Ubiquitous Blood Pressure Monitoring via Pulse Transit Time: Predictions on Maximum Calibration Period and Acceptable Error Limits, IEEE Transactions Biomedical Engineering 65 (6). doi:10.1109/TBME.2017.2756018

[3] M. P. Neves, A. W. Porto Jr., P. H. Souza, T. M. Barbosa. A Photoplethysmographic Monitor for Local Pulse Wave Velocity Measurement, International Journal of Computer Applications 177(31) (2020) 62-67. doi:10.5120/ijca2020919811

[4] R. Mukkamala, J.-O. Hahn, O. T. Inan, L. K. Mestha, C.-S. Kim, H. Töreyin, S. Kyal, Towards Ubiquitous Blood Pressure Monitoring via Pulse Transit Time: Theory and Practice, IEEE Transactions on Biomedical Engineering 62 (8) (2015) 1879–1901. doi:10.1109/TBME.2015.2441951

[5] D. J. McDuff, J. Hernandez, S. Gontarek, R. W. Picard, COGCAM: Contact-free Measurement of Cognitive Stress During Computer Tasks with a Digital Camera, in 2016 Conference on Human Factors in Computing Systems, San Jose, (2016) 4000–4004. doi:10.1145/2858036.2858247

[6] D. McDuff, S. Gontarek, R. Picard, Remote measurement of cognitive stress via heart rate variability, in 2014 36th Annual International Conference of the IEEE Engineering in Medicine and Biology Society, 26-30 Aug. 2014, Chicago, IEEE, 2014. doi:10.1109/EMBC.2014.6944243

[7] M.-Z. Poh, D. J. McDuff, R. W. Picard, Non-contact, automated cardiac pulse measurements using video imaging and blind source separation, Optics Express 18 (10) (2010) 10762–10774. doi:10.1364/OE.18.010762

[8] M.-Z. Poh, D. J. McDuff, R. W. Picard, Advancements in Noncontact, Multiparameter Physiological Measurements Using a Webcam, IEEE Transactions on Biomedical Engineering 58 (1) (2011) 7–11. doi:10.1109/TBME.2010.2086456

[9] N. Sugita, K. Obara, M. Yoshizawa, Techniques for estimating blood pressure variation using video images, in 2015 37th Annual International Conference of the IEEE Engineering in Medicine and Biology Society (EMBC), (2015) 25-29, Milan, Italy, IEEE, doi:10.1109/EMBC.2015.7319325

[10] E. Dolan, A. Stanton, L. Thijs, K. Hinedi, N. Atkins, S. McClory, et al., Superiority of ambulatory over clinic blood pressure measurement in predicting mortality: the Dublin outcome study, Hypertension, 46, (2005) 156-161. doi:10.1161/01.HYP.0000170138.56903.7a

[11] Y. L. Zheng, X. R. Ding, C. C. Poon, B. P. Lo, H. Zhang, X. L. Zhou, Unobtrusive sensing wearable devices for heart informatics, IEEE Transactions on Biomedical Engineering, 61(5) (2014) 1538-54. doi:10.1109/TBME.2014.2309951

[12] B. Klaassen, B. J. F. van Beijnum, H. J. Hermens, Usability in telemedicine systems—A literature survey, International Journal of

Medical Informatics, 93(9) (2016), 57-69. doi:10.1016/j.ijmedinf.2016.06.004

[13] M, Nitzan. B. Khanokh, and Y, Slovik, The difference in pulse transit time to the toe and finger measured by photoplethysmography, Physiological measurement, 23(8)5, (2001). doi:10.1088/0967-3334/23/1/308

[14] W. L. Khong, N. S. V. K. Rao, M. Mariappan, Blood pressure measurements using non-contact video imaging techniques: IEEE 2nd International Conference on Automatic Control and Intelligent Systems (I2CACIS), Kota Kinabalu, Malaysia, IEEE, 2017. doi:10.1109/I2CACIS.2017.8239029

[15] S. Laurent, J. Cockcroft, L. Van Bortel, P. Boutouyrie, C. Giannattasio, D. Hayoz, B. Pannier, C. Vlachopoulos, I. Wilkinson, H. Struijker-Boudier, Expert consensus document on arterial stiffness: methodological issues and clinical applications, European Heart Journal, 27(21) 2588-2605, 2006. doi:10.1093/eurheartj/ehl254

[16] X. R. Ding, N. Zhao, G. Z. Yang, R. I. Pettigrew, B. Lo, F. Miao, Y. Li, J. Liu, Y. T. Zhang, Continuous Blood Pressure Measurement from Invasive to Unobtrusive: Celebration of 200th Birth Anniversary of Carl Ludwig, IEEE Journal of Biomedical and Health Informatics, 20, 1455-1465, 2016. doi:10.1109/JBHI.2016.2620995

[17] T. P. Sacramento, I. M. B. Souza, P. V. O. Vitorino, T. M. G. A. Barbosa, A real-time software to the acquisition of heart rate and photoplethysmography signal using two regions of interest simultaneously via webcam, in 2017 IEEE MIT Undergraduate Research Technology Conference (URTC), (2017) 3-5 , Cambridge, MA, IEEE, 2018. doi:10.1109/URTC.2017.8284207

[18] M. P. Tarvainen, P. O. Ranta-aho, P. A. Karjalainen, An advanced detrending method with application to HRV analysis, IEEE Transactions on Biomedical Engineering 49 (2) (2002) 172–175. doi:10.1109/10.979357

[19] S. Kwon, H. Kim, K. S. Park, Validation of heart rate extraction using video imaging on a smartphone's built-in camera system, in 2012 Annual International Conference of the IEEE Engineering in Medicine Biology Society, 28 (1) 2012, San Diego, IEEE, doi:10.1109/EMBC.2012.6346392

[20] P. H. B. Souza, J. O. Ferreira, T. M. G. de A. Barbosa, A. F. da Rocha, HRVCam: A software for real-time feedback of heart rate and HRV, in 2016 IEEE 6th International Conference on Computational Advances in Bio and Medical Sciences (ICCABS), (2016) 13-15, Atlanta, IEEE, 2017. doi:10.1109/ICCABS.2016.7802767

[21] P. H. de B. Souza, I. M. B. Souza, T. P. Sacramento, P. C. de Matos Lima Martins, P. V. de Oliveira Vitorino, G. C. Ramos, T. M. G. de Andrade Barbosa, A. F. da Rocha, Contributions to the Acquisition of Heart Rate and Photoplethysmography Signal Using a Real-Time Software, in 2018 IEEE International Conference on Healthcare Informatics (ICHI), (2018) 4-7, 332–337. doi:10.1109/ICHI.2018.00046

[22] Gupta, R. K. Agrawal, B. Kaur, Performance enhancement of mental task classification using EEG signal: a study of multivariate feature selection methods, Methodologies, and Applications 19 (10) (2015) 2799–2812. doi:10.1007/s00500-014-1443-1

[23] S. G. Soares, R. Araújo, An Adaptive Ensemble of On-line Extreme Learning Machines with Variable Forgetting Factor for Dynamic System Prediction, Neurocomputing 171 (2016) 693–707. doi:10.1016/j.neucom.2015.07.035

[24] W. C. Tsai, J.Y. Chen, M.C. Wang, H.T. Wu, C.K. Chi, Y.K. Chen, J. H. Chen, L. J Lin, Association of risk factors with increased pulse wave velocity detected by a novel method using dual-channel photoplethysmography, American Journal of Hypertension, 18, 1118-1122, 2005. doi:10.1016/j.amjhyper.2005.03.739

[25] T. B. Fitzpatrick. The validity and practicality of sun-reactive skin types I through VI. Archives of Dermatology. 1988 Jun;124(6):869-871. doi:10.1001/archderm.1988.01670060015008

[26] L. M. da Silva, P. H. de B. Souza, A. F. da Rocha, T. M. G. de A. Barbosa. Contactless Cardio Monitor: a Contactless Cardiovascular Monitoring Software, International Journal of Biotech Trends and Technology 10(4) (2020) 30-37. doi: 10.14445/22490183/IJBTT-V10I4P604